The Astrophysical Journal, 718:266–278, 2010 July 20 doi:10.1088/0004-637X/718/1/266

ORIGIN OF CORONAL SHOCK WAVES ASSOCIATED WITH SLOW CORONAL MASS EJECTIONS

J. Magdalenić[1,2], C. Marqué[1], A. N. Zhukov[1,3], B. Vršnak[2], and T. Žic[2]
[1] Solar Terrestrial Center of Excellence-SIDC, Royal Observatory of Belgium, Av. Circulaire 3, B-1180 Brussels, Belgium; Jasmina.Magdalenic@oma.be
[2] Hvar Observatory, Faculty of Geodesy, Kačićeva 26, HR-10000 Zagreb, Croatia
[3] Skobeltsyn Institute of Nuclear Physics, Moscow State University, 119992 Moscow, Russia
Received 2009 December 23; accepted 2010 May 24; published 2010 June 29

ABSTRACT

We present a multiwavelength study of five coronal mass ejection/flare events (CME/flare) and associated coronal shock waves manifested as type II radio bursts. The study is focused on the events in which the flare energy release, and not the associated CME, is the most probable source of the shock wave. Therefore, we selected events associated with rather slow CMEs (reported mean velocity below 500 km s^{-1}). To ensure minimal projection effects, only events related to flares situated close to the solar limb were included in the study. We used radio dynamic spectra, positions of radio sources observed by the Nançay Radioheliograph, *GOES* soft X-ray flux measurements, Large Angle Spectroscopic Coronagraph, and Extreme-ultraviolet Imaging Telescope observations. The kinematics of the shock wave signatures, type II radio bursts, were analyzed and compared with the flare evolution and the CME kinematics. We found that the velocities of the shock waves were significantly higher, up to one order of magnitude, than the contemporaneous CME velocities. On the other hand, shock waves were closely temporally associated with the flare energy release that was very impulsive in all events. This suggests that the impulsive increase of the pressure in the flare was the source of the shock wave. In four events the shock wave was most probably flare-generated, and in one event results were inconclusive due to a very close temporal synchronization of the CME, flare, and shock.

Key words: shock waves – Sun: corona – Sun: coronal mass ejections (CMEs) – Sun: flares – Sun: radio radiation

1. INTRODUCTION

The energy release during the flare/coronal mass ejection (CME) process leads to the formation of large-amplitude coronal disturbances and shock waves. The longest-known signatures of shock waves are type II radio bursts (Wild 1950; Wild et al. 1954; Nelson & Melrose 1985). They appear in the dynamic radio spectrum as slowly drifting lanes of enhanced emission, generated at the local plasma frequency and/or its harmonics. Metric-wavelength type II bursts appear typically at or below 100 MHz, and they are caused by shocks traveling through the solar corona. Type II bursts recorded in the decameter-to-kilometer wavelength range are excited by shocks traveling through the upper corona and interplanetary space.

The origin of coronal shock waves is still not completely understood. Two possible physical explanations are a blast wave ignited by the pressure pulse of a flare, or, alternatively, a piston-driven shock due to a CME. While most of the interplanetary shocks are CME-driven, coronal shock waves can be attributed to solar flares, CMEs, or some combination of these phenomena (e.g., Reiner et al. 2001; Oh et al. 2007; Magdalenić et al. 2008; Vršnak & Cliver 2008).

Flares, CMEs, and shock signatures are usually closely temporally associated, and the association rate increases with the flare importance (Vršnak & Cliver 2008). Due to the close synchronization of the acceleration phase of the CME and the flare impulsive phase (Zhang et al. 2001; Maričić et al. 2007; Temmer et al. 2008), it is difficult to determine the origin of coronal shocks, i.e., metric type II bursts, on the basis of the CME and shock wave kinematics.

In recent years, a number of case studies provided examples of metric type II burst signatures of coronal shocks that were driven by CMEs (e.g., Raymond et al. 2000; Mancuso et al. 2002; Ciaravella et al. 2005), supporting the idea that all coronal shocks are CME-driven, as suggested by Cliver et al. (2004). The aim of our study is to test this hypothesis by trying to identify events where the shock wave cannot be attributed to the CME, but is caused by the flare energy release, similarly to the case study by Magdalenić et al. (2008). Consequently, for the analysis we selected events associated with relatively slow CMEs, since fast and wide CMEs are in general considered as shock wave drivers (Gopalswamy et al. 2008). To minimize projection effects, only close-to-limb and limb events were studied. The analysis is based on the comparison of the kinematics of the shock wave signature with the dynamics of the associated CME and the evolution of the flare energy release. Additionally, the measurements are compared with results of the theoretical model by Žic et al. (2008), who considered the three-dimensional piston scenario for the formation of large-scale disturbances in the solar corona. The observations and methods applied in the paper are presented in Section 2. The events are described in Section 3. The description of each event is followed by a brief discussion. Our conclusions are summarized in Section 4.

2. OBSERVATIONS AND METHODS

2.1. Observational Data

Type II radio bursts, i.e., signatures of coronal shock waves, were studied using high time resolution (0.1 s) dynamic spectra (Figure 1, left column) recorded by radiospectrographs of the Astrophysical Institute Potsdam (AIP; Mann et al. 1992). The AIP observations cover the frequency range 800–40 MHz. Positions of type II burst sources were determined using Nançay Radioheliograph (NRH; Kerdraon & Delouis 1997) observations at 432, 411, 327, 237, 164, and 151 MHz recorded with a time resolution of 0.5 s. To analyze radio signatures of the flare impulsive phase and to confirm the existence of metric type

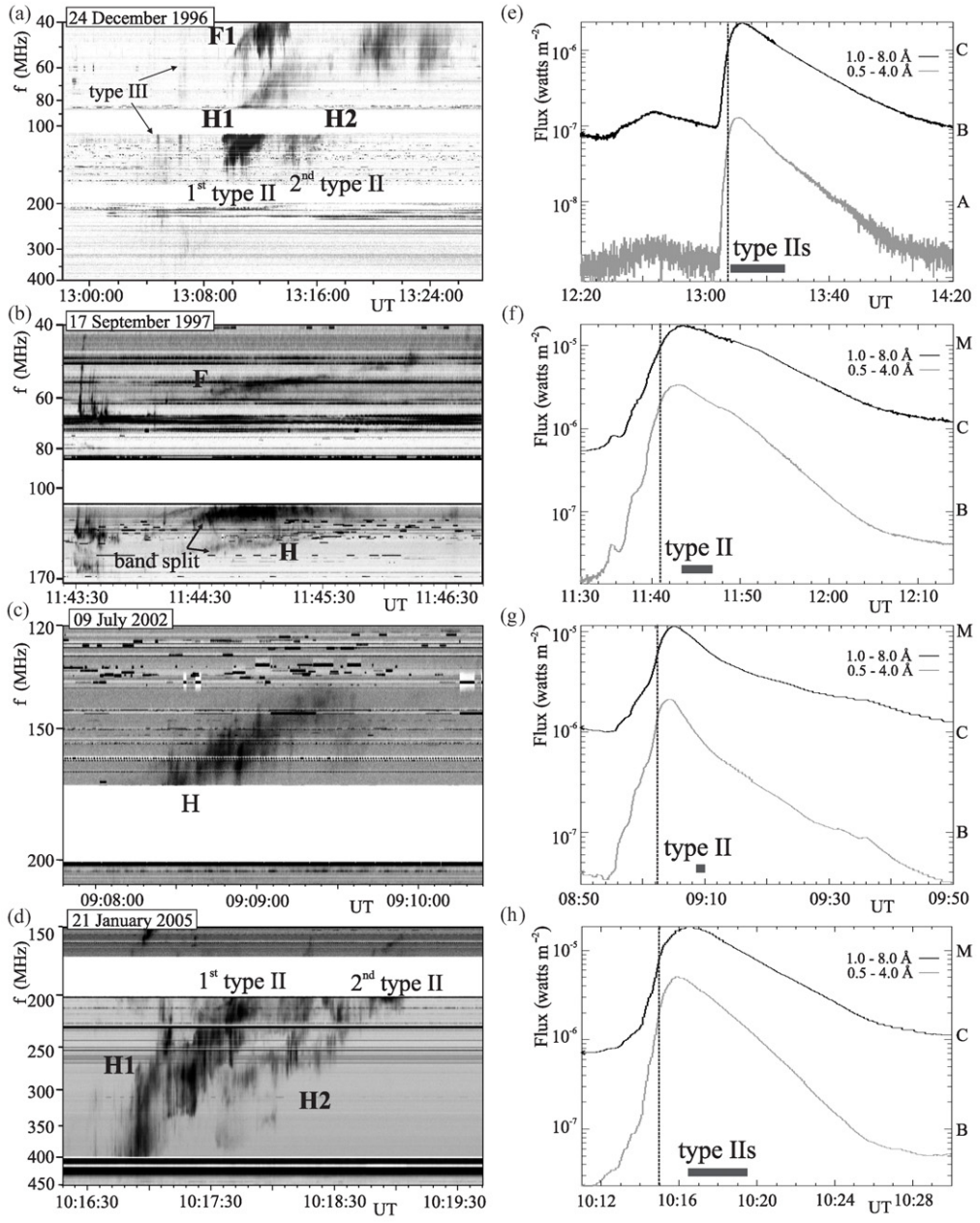

Figure 1. Left column: dynamic spectra recorded by the AIP spectrograph, showing selected metric type II bursts. Right column: *GOES* flare profiles with the black rectangle marking the duration of the type II emission, and the dotted line marking the maximum of the flare impulsive phase estimated using the Neupert effect. (a) Two homologous type II bursts recorded on 1996 December 24. Fundamental (F1) and harmonic (H1) emission bands of the first type II burst are both well defined, while the second type-II-like burst (H2) is rather patchy. (b) Fundamental and harmonic bands of the type II burst (F and H, respectively) recorded on 1997 September 17. (c) Harmonic band of type II burst recorded on 2002 July 9. (d) Harmonic bands of two homologous type II bursts (H1 and H2, respectively) recorded on 2005 January 21.

II bursts, we used dynamic spectra recorded by the broadband spectrometer Phoenix-2 (Messmer et al. 1999) in the frequency range of 4000–100 MHz.

Characteristics of associated flares were analyzed using *GOES* soft X-ray (SXR) flux measurements. Properties of CMEs were studied using the Large Angle Spectroscopic Coronagraph (LASCO; Brueckner et al. 1995) on board the *Solar and Heliospheric Observatory* (*SOHO*). For the analysis of the early stages of eruptions, we used observations provided by the Extreme-ultraviolet Imaging Telescope (EIT; Delaboudinière et al. 1995) with the field of view extending up to 1.4 $R_\odot$ from the solar disk center ($R_\odot$ is the solar radius).

2.2. Scaling of Coronal Density and Type II Velocity

As the frequency of radio emission depends on the local electron density, the height profile of the coronal density has the strongest influence on the interpretation of radio observations. Therefore, estimations of the radio-source height from the dynamic spectrum and its velocity depend on the choice of a density model. In the case of an eruption that appears close to the solar limb, the influence of the plane-of-the-sky projection effects is rather small. This characteristic provides the possibility to scale the density model using the NRH positions of radio sources (Magdalenić et al. 2008; Pohjolainen 2008). When

referring to the NRH position, we consider the position of the centroid of the radio source.

The procedure of the density-model scaling used for the events analyzed in our study is as follows. The evolution of the dominant radio source at the selected NRH frequency f was compared with the corresponding radio features in the AIP dynamic spectrum. The obtained position of the type II radio source (hereafter NRH source) was converted to the height above the photosphere H. To determine the electron density n_e, which corresponds to the frequency f, we employ the standard relationship $f \approx 9\,n_e^{1/2}$, where n_e is expressed in cm^{-3} and f in kHz. Comparing the radial dependence of the plasma density in different models (e.g., Newkirk 1961; Saito et al. 1970; Mann et al. 1999) with observations, we selected the most suitable model for the analyzed event. When the density model is obtained, the velocity of the shock wave can be estimated from the frequency drift of the type II burst.

The size of type II radio sources increases with the decrease of the observing frequency (Sheridan et al. 1973; McLean 1973; Magun et al. 1975). However, it does not show any systematic displacement of the radio-source centroid (L. Klein 2008, private communication). The observations show that the apparent positions of the fundamental and second/third harmonic sources at a given frequency generally coincide (Nelson & Melrose 1985; Aurass et al. 1994; Zlotnik et al. 1998). Therefore, we do not expect significant uncertainties in the height of the radio source estimated at lower NRH frequencies, e.g., 164 MHz, due to processes such as scattering, refraction, or ducting (see, e.g., Duncan 1979; Nelson & Melrose 1985).

2.3. Type II Band Split

Metric type II bursts usually show fundamental and harmonic emission bands. Both bands are often split in two parallel lanes of similar frequency drifts and intensity behavior (Nelson & Melrose 1985; Vršnak et al. 2001). The type II band split can be attributed to simultaneous emission from the plasma ahead of and behind the shock front, i.e., the upstream/downstream shock regions (Smerd et al. 1974, 1975; Vršnak et al. 2001).

According to the upstream/downstream hypothesis, the band split is a measure of the shock amplitude and can be used to estimate the Alfvén Mach number and the Alfvén speed (Vršnak et al. 2001, 2002, 2004a). In front of the shock wave, the plasma is characterized by the electron density n_L and emits radio waves at the frequency f_L. The density of the compressed plasma behind the shock is $n_H > n_L$, corresponding to the frequency $f_H > f_L$. Thus, the relative band split $\mathrm{BDW} = (f_H - f_L)/f_L$ defines the density jump at the shock front, $X \equiv n_H/n_L = (\mathrm{BDW}+1)^2$. In the following, we apply the perpendicular-shock approximation and plasma beta $\beta = 0$, where the Alfvén Mach number is related to the compression X as $M_A^2 = (X(X+5))/2(4-X)$ (Priest 1982). Finally, with the shock speed v_s obtained from the frequency drift, we can find the Alfvén velocity $v_A = v_s/M_A$ (for details of the procedure and a discussion of the applied approximations, we refer to Vršnak et al. 2002, 2004a; Magdalenić et al. 2008). For possible errors in the estimation of the type II drift rate, relative bandwidth, and accordingly Alfvén speed and Alfvén Mach number, see, e.g., Mann et al. (1995, 1996), and Vršnak et al. (2001).

2.4. The Neupert Effect

In a large number of solar flares, the time integral of the microwave and hard X-ray emission rather closely matches the rising part of the SXR emission. This is known as the Neupert effect (Neupert 1968; Veronig et al. 2002; Brown & Kontar 2005). Although, the match in timing is not always exact due to the integration effects in the SXR data and probably different physics, the Neupert effect can be used to estimate the timing of the flare impulsive phase that marks the time of the strongest energy release. In the studied events, the Neupert effect was used to define the flare impulsive phase by considering the time derivative of the SXR flux (*GOES* light curve at 1–8 Å).

2.5. Analytical MHD Model of Shock Formation

The observational results on the CME and shock kinematics were compared to the analytical MHD model proposed by Žic et al. (2008), which considers the formation of the shock wave by an impulsively expanding three-dimensional piston.[4] The model is based on the theory of nonlinear evolution of large-amplitude fast-mode magnetosonic waves in a planar, cylindrical, and spherical geometry. It follows the steepening of the wave profile until the appearance of the discontinuity, i.e., the shock. The input parameters of the model are the maximum velocity of the source-region surface (the piston), the acceleration-phase duration, the initial piston size, and the ambient Alfvén velocity. The model by Žic et al. (2008) shows that the shock formation time and shock formation distance are most directly dependent on the duration of the source region acceleration dt_{acc}, i.e., the duration of the acceleration phase of a CME.

In this study, it was possible to estimate the duration of the CME acceleration in only one event (1996 December 24). We found that the CME acceleration lasted about $dt_{\mathrm{acc}} \approx 28$ minutes. It should be noted that due to the limited time resolution of the LASCO observations the estimated value was possibly an upper-limit value. To assure the most favorable conditions for the CME as a possible driver of the shock wave, for the input to the theoretical model we considered the duration of the CME acceleration only from the beginning to the maximum of the CME acceleration. This amounts to about one-half of the total duration of the CME acceleration ($1/2\,dt_{\mathrm{acc}} \approx 14$ minutes). A broad range of the acceleration phase durations was reported in the literature (see, e.g., Zhang & Dere 2006; Vršnak et al. 2007; Temmer et al. 2008, 2010). As a result of an extensive statistical study, Zhang & Dere (2006) reported the duration of the acceleration phase to be in the range of 6–1200 minutes. To our knowledge, the acceleration phase lasting only for 6 minutes is the shortest one ever reported. Due to the lack of observations of the complete CME acceleration phase for the majority of presented events, we used values of $dt_{\mathrm{acc}} = 5$, 10, and 15 minutes as an input to the theoretical model. The acceleration phase lasting $dt_{\mathrm{acc}} = 5$ minutes is even shorter than the shortest one reported (6 minutes; Zhang & Dere 2006). In this way, the most favorable conditions for the CME to drive the observed shock were considered. The values of $dt_{\mathrm{acc}} = 10$ minutes and $dt_{\mathrm{acc}} = 15$ minutes are close to the observed value for the 1996 December 24 event ($1/2\,dt_{\mathrm{acc}} \approx 14$ minutes). We note that the shorter acceleration time corresponds to the faster shock formation.

The majority of CME/flare events show rather good synchronization of the flare impulsive phase and the CME acceleration phase (Zhang & Dere 2006; Maričić et al. 2007; Temmer et al. 2008, 2010). Although the flare impulsive phase is usually shorter than the CME acceleration (Maričić et al. 2007; Temmer et al. 2010), it can be considered as a measure for

[4] The model by Žic et al. (2008) is a generalization of the one-dimensional model by Vršnak & Lulić (2000).

Table 1
Characteristics of Flares, CMEs, and Type II Radio Bursts Associated with the Selected Events

Date	Soft X-ray Flare	Flare Location	Flare	Flare Impulsive Phase[a]	First CME	CME Speed		Type II
	Start–Peak–End	on the Disk	Importance	Start–Peak–End	Signatures	Catalog	Estimated[b]	Speed[c]
(dd.mm.yyyy)	(UT)			(UT)	(UT)	(km s^{-1})	(km s^{-1})	(km s^{-1})
24.12.1996	13:05–13:11–14:20	6°N 85°W	C 1.1	13:04–13:06–13:11	13:14 (EIT)	325	110 ± 30	1100 ± 15
17.09.1997	11:35–11:43–12:12	21°N 82°W	M 1.7	11:38–11:41–11:43	11:39 (C1)	447	240[d] ± 30	680 ± 10
09.07.2002	08:54–09:05–09:50	24°N 89°W	M 1.0	09:01–09:03–09:05	09:12 (EIT)	276	250 ± 30	1140 ± 40
21.01.2005	10:12–10:16–10:30	19°N 81°W	M 1.7	10:14–10:15–10:16	10:29 (EIT)	273	220 ± 50	2100 ± 80
16.04.2002	10:37–10:44–11:20	14°S 77°W	C 9.3	10:39–10:41–10:44	11:00 (EIT)	496	600[e] ± 30	1000[f] ± 20

Notes.
[a] The timing of the flare impulsive phase, which marks the time of the strongest energy release, was estimated using the Neupert effect (Neupert 1968).
[b] The CME velocity was measured in the LASCO C1 field of view for the 1996 December 24 event, and in the LASCO C2 field of view for all other events. The CME error bars in the speed were obtained using the errors in the position of the leading edge of the CME.
[c] The error bars of the shock speed were estimated using different density models.
[d] Two CMEs were observed in this CME/flare event with speeds of 390 and 240 km s^{-1}. The shock wave seems to be associated with the second (slower) CME.
[e] The CME decelerates from 600 to 500 km s^{-1}.
[f] The shock wave seems to decelerate from 1000 to 300 km s^{-1}.

the CME impulsive acceleration phase. The shortest acceleration phase considered as an input to the theoretical model $dt_{\rm acc} = 5$ minutes is of the same order of magnitude as the flare impulsive phase duration (Table 1).

3. ANALYSIS OF CME/FLARE EVENTS

We inspected a large number of CME/flare events to select well-observed cases. The selection criteria were: (a) reported signatures of coronal shock waves—metric type II radio bursts; (b) existence of NRH observations; (c) limb events, i.e., the flare location more than 60° from the solar central meridian; and (d) existence of coronagraph data and association with rather slow CMEs, i.e., the mean CME speed reported in the LASCO catalog (Yashiro et al, 2004) $v_{\rm CME} \leqslant 500$ km s^{-1}.

The five selected events, which fulfill the imposed criteria, are listed in Table 1. The table contains information about the timing of the SXR flare, flare location on the disk, and its importance in Columns 2, 3, and 4, respectively. The fifth column shows the time interval of the flare impulsive phase estimated using the Neupert effect (Neupert 1968). The time of the first observed CME signatures and the reported mean CME velocity in the LASCO field of view are listed in Columns 6 and 7, respectively. The CME speed estimated for the time interval closest to the appearance of the type II burst and the shock speed estimate from the type II burst drift rate are listed in Columns 8 and 9, respectively.

3.1. The 1996 December 24 Event

3.1.1. Characteristics of the Flare and Radio Event

The event on 1996 December 24 was related to a *GOES* C2.1 flare from the NOAA AR 8007/8004 (5°N 74°W/6°N 85°W). The associated flare started at 13:05 UT and attained its maximum at 13:11 UT (Figure 1(e) and Table 1).

The intense, fast drifting type-III-like bursts observed in the microwave range (4.5–2.0 GHz) at 13:04:30–13:09:00 UT indicate the impulsive phase of the flare. In the same time interval, faint metric type-III-like bursts were also observed. In Figure 1(a), due to background subtraction used to emphasize more intense type II bursts, metric type-III-like bursts are almost invisible.

Two metric type II bursts were observed between 13:09 and 13:26 UT (denoted in Figure 1(a) as first and second type II). The first type II burst shows both fundamental and harmonic emission bands (denoted as F1 and H1). The harmonic band is better defined than the fundamental one, and is split in two lanes (Nelson & Melrose 1985; Vršnak et al. 2001). After the first type II burst, a faint second type-II-like burst is observed. The high-frequency part of the second type II burst is homologous to the first type II harmonic band (Figure 1(a)) which indicates that this is also probably the harmonic emission. The conclusion is supported by the facts that we do not observe type II emission at the double frequency, and that in metric type II bursts harmonic emission is usually stronger than the fundamental (Vršnak et al. 2001). The observed morphological similarities between the two type II bursts indicate that both shocks passed through coronal structures of similar characteristics (and thus the same density model can be used for both type II bursts). For more details, see Figure 1 in Magdalenić et al. (2008). Both type II bursts show a similar drift rate of $df/dt = 0.2$ MHz s^{-1} indicating that the shock velocities were also similar.

With a starting frequency of 170 MHz (close to the lowest observing frequency of the NRH), only the first type II source location could be identified. The position of the 164 MHz NRH source[5] (type II harmonic band), which corresponds to the plasma frequency $f = 164/2 = 82$ MHz, was found to be at $R = 1.4\,R_\odot$. According to the procedure described in Section 2.2, the most suitable density model for this event is 3.5× Saito (Figure 2). When considering the most extreme positions of the NRH source, the densities of 3.2× Saito and 3.6× Saito were obtained. Using the "average" coronal density model 3.5× Saito and the frequency drift of the type II burst, we obtained a type II velocity of about $v_s \approx 1100$ km s^{-1}. The error on the shock speed estimation using the density models of 3.2× and 3.6× Saito is rather small (±15 km s^{-1}). Due to a rather exact estimation of the density model, the errors in the estimation of the shock speed caused by the usage of different density models are rather small. The same conclusion holds for all of the studied events. Using the measured band split (BDW $\approx$ 0.26) of the type II burst, we found the Alfvén Mach number and Alfvén velocity to be 1.56 and 700 km s^{-1}, respectively. More details about this event can be found in Magdalenić et al. (2008).

[5] The estimated position of the NRH source is an average value of multiple measurements. The error bars (Figure 2) reflect the dispersion of the individual measurement with respect to the average position of the centroid of the NRH source.

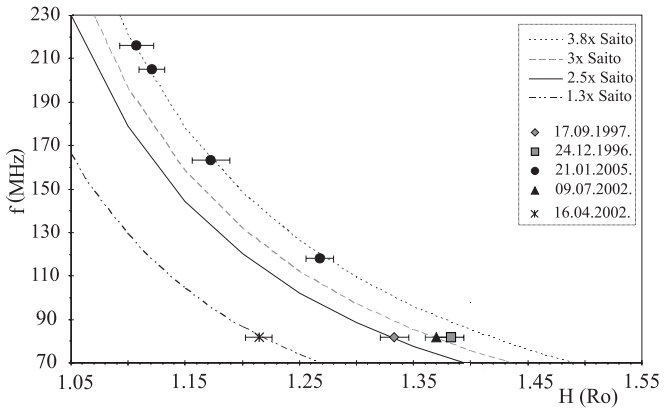

Figure 2. Positions of centroids of the radio sources obtained from NRH observations converted to radio-source heights H and shown as a function of the NRH observing frequency f. The data are compared with the Saito density model (Saito et al. 1970).

3.1.2. CME and Associated Dynamics in the Low Corona

Base difference EIT (195 Å bandpass) images in Figure 3(a) show early signatures of the CME associated with the 1996 December 24 event. A rising pre-eruption structure is already visible in the EUV at 13:02:20 UT. Signatures of the CME were clearly observed only at 13:14:14 UT. EIT running-difference images show signatures of the EIT wave propagating southward from the active region (Figure 3(b)) with a velocity of about 250 km s^{-1}.

To reveal the plane-of-the-sky position of the NRH type II source relative to the CME, we overlaid the contours of the NRH source (corresponding to the harmonic band of the first type II burst), on the EIT image (Figure 3(c)). Since the EIT image is recorded at 13:14:14 UT and the NRH source at 13:10:07 UT, a correction in the position of the NRH source is needed. The corrected position of the NRH source was estimated taking into account the average velocity of the type II and the time difference between two images (1100 km s^{-1} and 4.12 minutes, respectively). After corrections, at 13:14:14 UT the NRH source appears to be about 300–360 Mm in front of the CME leading edge.

The CME was observed in the LASCO C1 field of view at 13:20 UT and in the LASCO C2 field of view at 13:28 UT (Figure 3(d)). The height of the CME leading edge was measured at several position angles to get an estimate of the measurement errors. Additionally, the CME leading edge was rather well defined and we took into account the error of measurement of ±2 pixels in both EIT and LASCO C1 fields of view and obtained the error in the position of about $\pm 0.005\,R_\odot$ and $\pm 0.01\,R_\odot$, respectively. The error bars are smaller than the plotting symbol size in Figure 3(e). Using the average CME heights, we find the mean CME velocity in the time intervals 13:02–13:14 UT, 13:14–13:20 UT, 13:20–13:28 UT, and 13:28–13:58 UT to be 110, 560, 1110, and 500 km s^{-1},

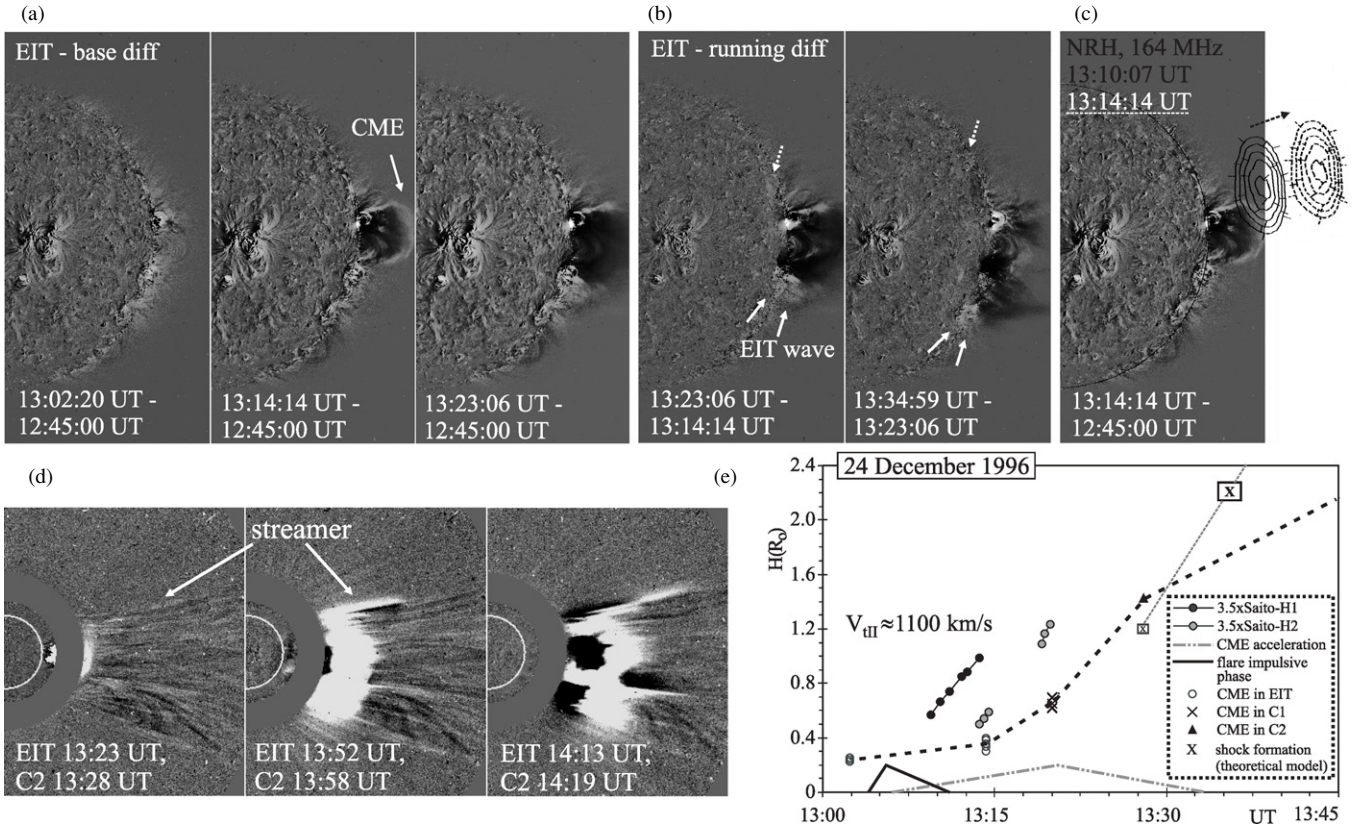

Figure 3. CME/flare event on 1996 December 24. (a) Base difference *SOHO*/EIT 195 Å images (the last pre-event image is subtracted from other images) show early CME signatures. (b) The EIT wave (marked with arrows) shown in EIT running-difference images (the previous image of a sequence is subtracted from every image). (c) The NRH radio source imaged at 13:10:07 UT (solid contours), corresponding to the harmonic band of the first type II burst, overlaid on the EIT image taken at 13:14:14 UT. The time-corrected position of the NRH source is marked with dashed contours. (d) *SOHO*/LASCO C2 running-difference images combined with temporally closest EIT running-difference images show the propagation of the CME. (e) Kinematics of the CME (dashed line) compared with signatures of the shock wave. The position of the shock formation, estimated with the theoretical model by Žic et al. (2008), for the duration of the acceleration phases of 5 minutes and 10 minutes is marked with "x" and "X," respectively. The y-axis represents the height above the photosphere.

respectively. We do not know when exactly the pre-erupting structure visible in the EIT image at 13:02 UT actually started to rise. Therefore, the CME speed of 110 km s^{-1} is a lower limit speed. If we consider that the eruption started at the time of the first appearance of the type II burst (13:02 UT), the obtained CME speed would be only a little higher (190 km s^{-1}).

The mean CME speed reported in the LASCO CME catalog (Yashiro et al. 2004), 325 km s^{-1}, is the average speed in the LASCO C2 and C3 fields of view. It is comparable with the average speed obtained for the time interval of interest, i.e., during the type II burst (13:09–13:20 UT). For a more detailed discussion of this event, we refer to Magdalenić et al. (2008).

A comparison of the CME and the shock wave kinematics is shown in Figure 3(e). The flare impulsive phase and the CME acceleration (in Figure 3(e), denoted as a black and gray dash-dotted triangle, respectively) do not coincide in time, i.e., in this event the flare and CME are not synchronized (for similar events, see Maričić et al. 2007). The acceleration of the CME peaked at 13:20:30 UT, which is about 10 minutes after the end of the impulsive phase of the flare, and ended around 13:33:28 UT. The CME acceleration reached its maximum about 7 minutes after the onset of the second type-II-like burst emission. Furthermore, the velocity of the type II bursts (1100 km s^{-1}) was about an order of magnitude larger than the contemporaneous CME velocity (110 ± 20 km s^{-1}). On the other hand, back-extrapolation of both type II bursts fits well with the flare impulsive phase, indicating that the shock waves might have been generated by the explosive energy release in the flare.

In this CME/flare event, the velocity of the CME is sub-Alfvénic and it strongly differs from the shock wave speed. Therefore, we can exclude the bow-shock scenario as the mechanism of the shock formation. We now compare the observational results with the theoretical three-dimensional piston scenario (Žic et al. 2008). The CME acceleration phase observed clearly only in this event lasts about $dt_{\rm acc} = 14$ minutes. However, due to the limited time resolution of the EIT and LASCO observations, it can be considered as an upper-limit value. We used three different durations of the acceleration phase: $dt_{\rm acc} = 5$, $dt_{\rm acc} = 10$, and $dt_{\rm acc} = 15$ minutes. The same procedure was done for all studied events. The detailed results are listed for $dt_{\rm acc} = 5$ minutes (10 minutes). The position of the shock formation for $dt_{\rm acc} = 15$ minutes is out of the range of Figure 3(e), and we do not regard it as relevant. We consider that the CME accelerates from 0 to 250 km s^{-1}, which gives an average velocity of 125 km s^{-1}. The average velocity considered in the theoretical model is approximately equal to the observed CME velocity in the interval of interest. According to the theoretical three-dimensional piston scenario, with an initial piston size of 100 Mm, and with an ambient Alfvén velocity of 700 km s^{-1} (as obtained from the band split), the shock would form in about 18 (37) minutes at the distance of 750 (1450) Mm (about 1 $R_\odot$ (2 $R_\odot$) above the first observed CME signatures). The modeled positions of the shock formation are marked in Figure 3(e) as "X." We note that the modeled shock formation occurs much higher than and long after the passage of the type II burst, even in the case when the most favorable conditions for the CME-driven shock were considered, i.e., $dt_{\rm acc} = 5$ minutes. We also note that, even if the earlier estimated higher CME speed of 190 km s^{-1} is considered, the conclusion does not change. In that situation, the modeled shock formation would be at slightly lower heights. However, due to a later start of the acceleration phase, the shock formation would also be "shifted" to later times. This would cause an even larger discrepancy between the time when the type II bursts appear and the time of the shock formation. We conclude that the CME cannot be considered as the driver of the shock wave, and that the shock waves in this event were probably generated by the flare. For more detailed consideration, see Magdalenić et al. (2008).

3.2. The 1997 September 17 Event

3.2.1. Characteristics of the Flare and Radio Event

The event on 1997 September 17 was related to a *GOES* M1.7 flare from the NOAA AR 8084 (21°N 82°W). The flare started at 11:35 UT, attained maximum at 11:43 UT, and ended at about 12:12 UT (Figure 1(f) and Table 1).

No microwave signatures were observed related to this event. In the metric range, around 11:39–11:40 UT, the AIP dynamic spectrum shows type-III-like bursts which indicate the impulsive phase of the associated flare. Slowly drifting emission bands of a metric type II burst were observed during 11:43:40–11:47:00 UT. Both fundamental and harmonic bands of the type II burst are well observed in the metric range (Figure 1(b)), but they do not extend to lower frequencies.

The harmonic band of the type II burst is more intense than the fundamental band and shows well-defined band split (BDW $\approx$ 0.23). The frequency drift of the type II burst df/dt is about 0.13 MHz s^{-1}. We identified that the NRH source at 164 MHz (corresponding to the harmonic band of the type II burst) was located at $R = 1.3\ R_\odot$. According to the procedure described in Section 2.2, the frequency level of $f = 164/2 =$ 82 MHz at the height of $R = 1.3\ R_\odot$ corresponds to a coronal density model of approximately 2.5× Saito (Figure 2). When the most extreme positions of the NRH source were considered, we obtained the densities of 2.3× Saito and 2.7× Saito. Using the average coronal density profile of 2.5× Saito and procedures described in Sections 2.2 and 2.3, we obtained the velocity of the shock wave, the Alfvén velocity, and the Alfvén Mach number to be $v_s \approx 680$ km s^{-1}, $v_A \approx 490$ km s^{-1}, and $M_A \approx 1.4$, respectively. The shock speed, estimated using the two similar density models (2.3× Saito and 2.7× Saito), differs only slightly (± 10 km s^{-1}).

3.2.2. CME and Associated Dynamics in the Low Corona

EIT observations at 195 Å show a rather slowly evolving trans-equatorial loop system (Figure 4(a)) connecting NOAA ARs 8084 (21°N 82°W) and 8085 (25°S 55°W). The eruption, involving not only the NOAA AR 8084 but also this trans-equatorial loop system, started concurrently with the impulsive phase of the flare at about 11:40 UT. The eruption was accompanied by a rather large coronal dimming, a spray-like southward-directed ejection of the dark (cold) material, a diffuse EIT wave (observed only at 11:57:50 UT), and weak signatures of post-eruption loops.

In the LASCO C1 field of view, a loop structure, possibly an early signature of the CME, was visible already at 11:39:11 UT. Figure 4(b) shows the NRH type II burst radio source overlaid on the temporally closest LASCO C1 image. We note that the NRH type II burst source was recorded about 4 minutes later than the LASCO C1 image, so a correction of the NRH source position in time would bring the NRH source even closer to the solar surface.

The LASCO CME catalog (Yashiro et al. 2004) reports the CME propagation velocity of 447 km s^{-1}. However, LASCO C2 images show the propagation of two subsequent

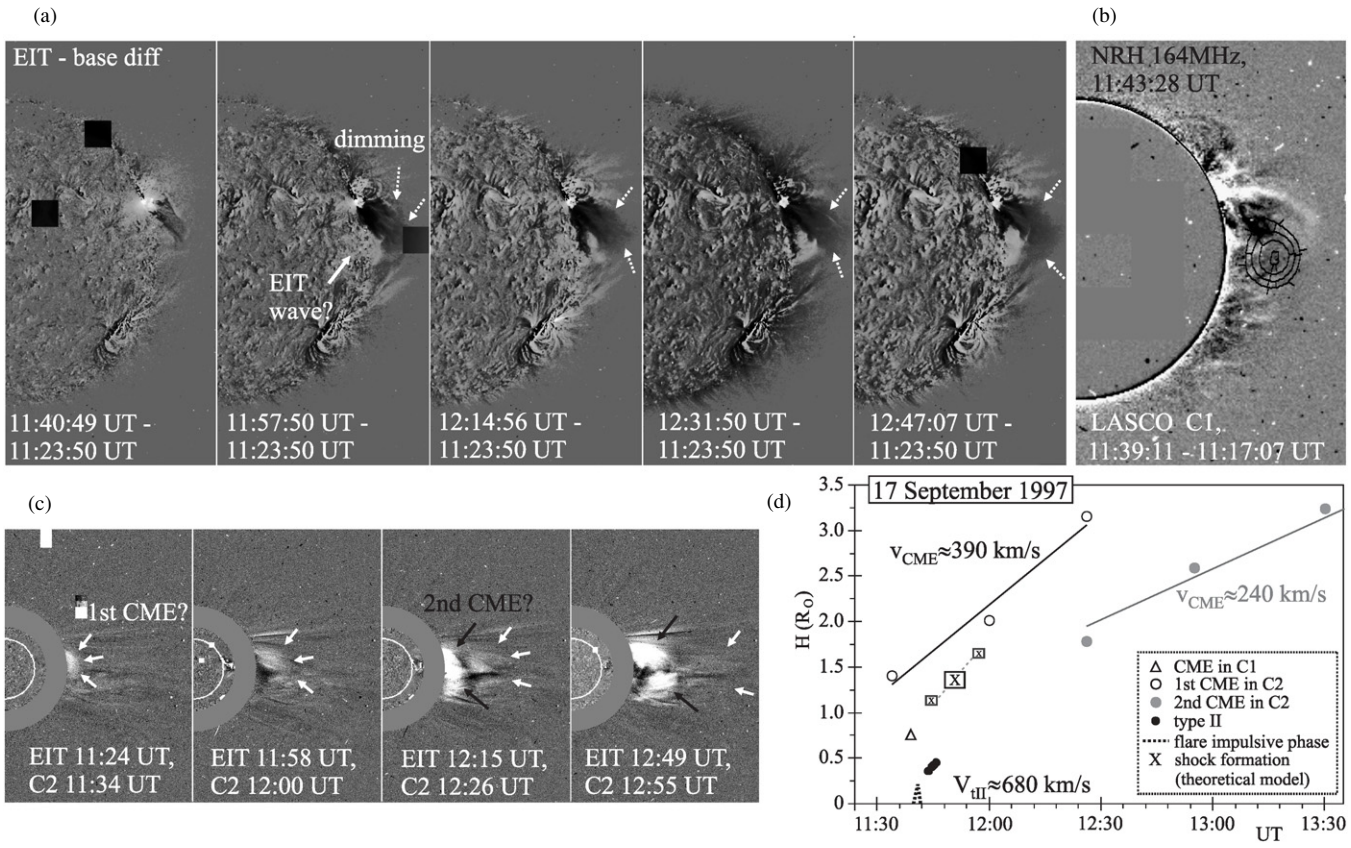

Figure 4. CME/flare event on 1997 September 17. (a) Base difference EIT images (the pre-event image is subtracted from other images) show the eruption of the trans-equatorial loop system, EIT wave signatures, and rather strong dimming (marked with dashed arrows). (b) LASCO C1 base difference image showing an erupting trans-equatorial loop system with the NRH type II burst source superposed. (c) LASCO C2 running-difference images of CMEs combined with temporally closest EIT running-difference images. First and second CMEs are marked with white and black arrows, respectively. (d) Kinematics of CMEs compared with signatures of the shock wave and flare. The position of the shock formation, estimated with the theoretical model by Žic et al. (2008), for the acceleration phase duration of 10 minutes is marked as "X." The shock formations estimated for the acceleration phase lasting 5 and 15 minutes are denoted with symbols "x." The *Y*-axis represents the height above the photosphere.

CMEs, or possibly two components of a single complex CME (Figure 4(c)). The kinematics of the two-part structure (or two CMEs) together with the shock wave signatures and the impulsive phase of the flare is shown in Figure 4(d). The CME dynamics indicate that we most probably observe two distinct mass ejections (hereafter first and second CMEs). The faint and rather diffuse leading edge of the first CME was first observed at 11:34 UT and could be clearly isolated only in three consecutive images. The CME velocity was about 390 km s^{-1}. At the time of appearance of the type II burst (i.e., the shock signature), the first CME was already at the height of 1.4 $R_{\odot}$, which is about 1 $R_{\odot}$ above the observed shock wave signatures (Figure 4(d)). In the scenario of a piston-driven shock wave, it is expected that the shock propagates ahead of the CME. If the shock wave is generated at the CME flanks, and not close to the CME nose, the height of the shock signatures would be smaller than the height of the CME nose. As the position of the NRH source is inside the angular span of the LASCO CME (Figure 4(b)), the possibility of the shock being on the CME flank is unlikely. Thus, we conclude that the first CME was not associated with the shock wave observed in this event.

The second CME appeared at 12:26 UT and initially had bright and well-contrasted structure (Figure 4(c)). Similarly to the first CME, the well-defined structure of the CME was smeared out relatively soon. The eruption and dimming observed by EIT seem to be related to this CME. The back-extrapolation of the second CME kinematics observed by LASCO C2 fits rather well with the height of the loop structure observed by LASCO C1. On the other hand, the same loop structure was at about 490 Mm below the first CME (Figure 4(d)). Therefore, we conclude that the loops observed by LASCO C1 were probably the low-height signature of the second CME. Since these loops were not clearly defined, when estimating the error of measurement of their height we took into account the error of ±4 pixels. The CME front was well defined in the LASCO C2 field of view, so the error of ±2 pixels was considered. The error in the estimated position of the CME leading edge was ±0.02 $R_{\odot}$ in both cases. These error bars are of the size of the plotting symbol size in Figure 4(d). The velocity of the second CME (calculated using the LASCO C2 observations) was found to be about 240 ±30 km s^{-1}, which is almost three times slower than the shock velocity (680 km s^{-1}).

In Figure 4(b), the NRH source is overlaid on the temporally closest LASCO C1 image, showing that the radio source was located at a much lower height than the leading edge of the erupting structure ($\Delta H \approx 270$ Mm). Moreover, since the NRH source was recorded about 4 minutes later than the LASCO C1 image, we conclude that the height difference between the CME leading edge and the shock signature was even larger (Figure 4(d)). This large discrepancy implies that the type II burst associated shock wave was not driven by the second CME either.

The CME and shock dynamics were compared with the analytical MHD model by Žic et al. (2008). The model was used to estimate the height and the time of the shock wave formation, presuming that it was driven by the second CME. As the input parameters to the model, we used an ambient Alfvén velocity obtained from the band split (490 km s^{-1}) and an initial piston size which is approximated by the size of the early CME signatures (about 100 Mm). We considered that the CME accelerates from 0 to 500 km s^{-1} (average velocity of 250 km s^{-1}) and that the acceleration starts at the moment of the first observation of the CME in the LASCO C1 field of view. Similarly to the previous event, we considered the duration of the acceleration phase of $dt_{acc} = 5$, $dt_{acc} = 10$, and $dt_{acc} = 15$ minutes. The positions of the shock formation estimated with the analytical model are marked in Figure 4(d) as "X". We discuss in more detail the results obtained for the $dt_{acc} = 5$ minutes (10 minutes). The result for $dt_{acc} = 15$ minutes does not make any additional contribution to the conclusion (see Figure 4(d)). The model shows that the shock wave would form about 6 (12) minutes after the onset of the CME acceleration and at the height of 270 (440) Mm from the initial CME position (in LASCO C1). The shock wave, if driven by this slow CME, would appear at significantly larger heights of about 0.8 $R_\odot$ (1 $R_\odot$) above the observed shock signatures (Figure 4(d)). Furthermore, at the time of the theoretically estimated shock formation, the observed shock signatures already disappeared. We note that the type II bursts appear at significantly lower heights and apparently after the CME acceleration phase. The shock does not seem to be CME-driven, even in the case when the most favorable situation for the CME-driven shock formation is considered ($dt_{acc} = 5$ minutes). Thus, we conclude that in this CME/flare event the shock wave was not caused by the CME expansion. On the other hand, the shock wave kinematics were very closely associated with the impulsive phase of the flare, so we conclude that the shock wave of the 1997 September 17 event was probably generated by the flare energy release.

We note that the modeled shock formation occurs much higher than and long after the passage of the type II burst, even in the case when the most favorable conditions for the CME were considered, i.e., $dt_{acc} = 5$ minutes.

3.3. The 2002 July 9 Event

3.3.1. Characteristics of the Flare and Radio Event

The CME/flare event on 2002 July 9 was related to a *GOES* M1.0 flare from the NOAA AR 10026 on the west limb (24°N 89°W). Characteristics of the SXR flare (Figure 1(g)) and its impulsive phase are listed in Table 1.

In the microwave range (4.5–2.0 GHz), no radio signatures associated with this CME/flare event were observed. A metric type II burst (Figure 1(c)) was observed at 09:07–09:11 UT in the frequency range of 210–120 MHz (AIP and Phoenix-2 dynamic spectra).

The comparison of the AIP dynamic spectrum (Figure 1(c)) and the NRH observations was possible only at 164 MHz. We found that the type II burst NRH source was located at a heliocentric distance of $R = 1.4\ R_\odot$, which corresponds to a coronal density model of 3× Saito. When the extreme positions of the NRH source were considered, we obtained the densities of 2.8× Saito and 3.3× Saito. The obtained density profiles were used to estimate the shock speed of 1140± 40 km s^{-1}. Additionally, from type II band split (BDW $\approx$ 0.13) we estimated the Alfvén velocity and Alfvén Mach number to be 940 km s^{-1} and 1.2, respectively.

3.3.2. CME and Associated Dynamics in the Low Corona

Figure 5(a) shows EUV (EIT, 195 Å) observations of the CME/flare event on 2002 July 9. First signatures of a slowly developing dimming were observed at 09:23:59 UT. At the same time, a weak dimming is observed in the active regions close to the southwest limb (NOAA 0019, 0021, and 0022). The height of the pre-erupting loop system (possible first signature of the CME) observed at 09:11:59 UT is marked by a triangle in Figure 5(d). Since the pre-erupting loops were not clearly defined, we considered the error of the measured height of ±4 pixels (±0.01 $R_\odot$). The error bars are smaller than the plotting symbol size in Figure 5(d).

Figure 5(b) shows the strongly elongated NRH type II burst source overlaid on the temporally closest EIT image (white contours). The corrected position of the NRH source (taking into account the shock velocity of 1140 km s^{-1} and the time difference of 3 minutes between EIT and NRH images) is denoted by black contours. We note that at 09:11:59 UT the corrected position of the type II burst source was located about 0.5 $R_\odot$ higher than the tip of the EUV structure. This indicates a very large standoff distance between the shock wave and its potential driver, the CME leading edge. If the shock wave would be generated at the CME flanks, the height of the shock signatures would be smaller than the height of the CME leading edge. This is not the case in our event. These findings do not favor the scenario of the CME-driven shock wave.

Figure 5(c) shows the evolution of the CME in LASCO C2 images. The mean CME speed of 276 km s^{-1} was reported in the LASCO CME catalog (Yashiro et al. 2004), which is very similar to the speed of 250 ± 30 km s^{-1} obtained in this study. We note that the error of ±4 pixels for the estimated position of the CME leading edge was considered. The error of ±0.05 $R_\odot$ is close to the size of the symbols in Figure 5(d).

Let us assume, for the sake of argument, that the CME initially had a velocity similar to the velocity of the shock wave and decelerated to the velocity observed in the LASCO C2 field of view. The CME deceleration would be as large as −270 m s^{-2}, which is more than the usually observed values (Vršnak 2001).

If the loop structures observed by EIT at 09:11:59 UT are an early signature of the CME, it can be considered that the acceleration starts at this moment and the observational results can be compared with the analytical MHD model (Žic et al. 2008). As an input to the theoretical model we used an initial piston size of about 100 Mm, an ambient Alfvén speed of 940 km s^{-1} (obtained from the band split), and an average CME speed of 250 km s^{-1} (acceleration from 0 to 500 km s^{-1}). Similarly to the previous events, we consider the duration of the acceleration phase of $dt_{acc} = 5$, $dt_{acc} = 10$, and $dt_{acc} = 15$ minutes. The model results obtained for the $dt_{acc} = 5$ minutes (10 minutes) are commented on in more detail, while the results for $dt_{acc} = 15$ minutes can be seen in Figure 5(d). The model results show that the shock wave would form about 11 minutes (22 minutes) after the onset of the CME acceleration at the height of 700 Mm (1250 Mm) above the possible initial CME position (as observed by EIT). The modeled positions of the shock formation (marked as "X" in Figure 5(d)) are also at significantly larger heights (about 0.5 $R_\odot$ (1.2 $R_\odot$)) than the observed shock signatures. Furthermore, the modeled shock formation is more than 10 minutes (20 minutes) after the appearance of the type II burst. The model results show that

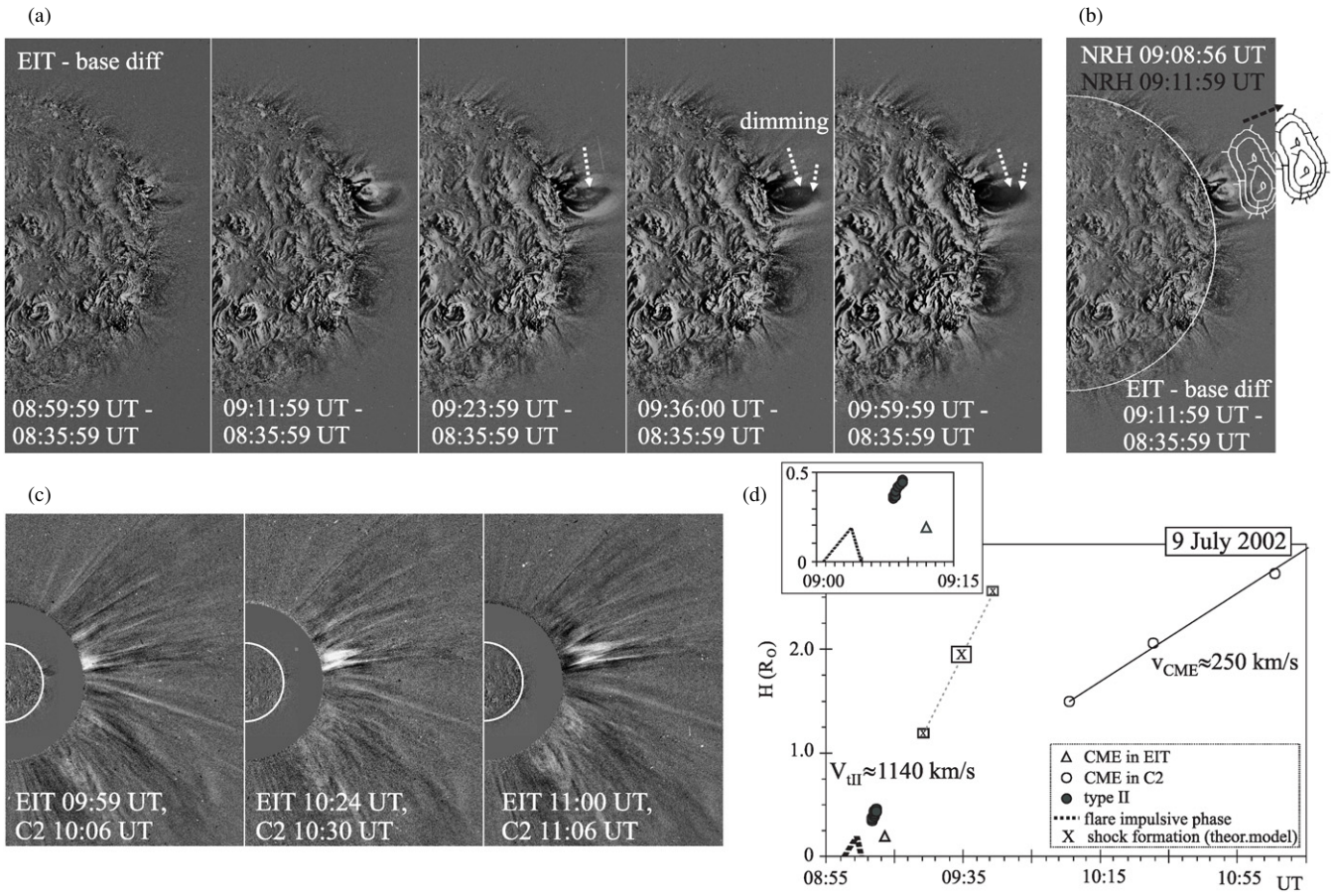

Figure 5. CME/flare event on 2002 July 9. (a) Base difference EIT images show a dimming (marked with dashed arrows). (b) The elongated radio source (marked with white contours) of the type II burst observed by the NRH at 164 MHz is overlaid on the closest EIT image (09:11:59 UT). The position of the NRH source was corrected taking into account the time difference between the shock signatures and the EIT image and the velocity of the shock (the corrected position is denoted with black contours). (c) LASCO C2 running-difference images combined with temporally closest EIT running-difference images show the CME propagation. (d) Kinematics of the CME compared with signatures of the shock wave and the flare impulsive phase. The position of the shock formation, estimated with the theoretical model, is marked as "X" for the acceleration phase duration of 10 minutes and as "x" for the acceleration phase duration of 5 and 15 minutes.

it is unlikely that the CME was the driver of the shock wave on 2002 July 9, not even when the most favorable conditions for the CME-driven shock formation were considered, i.e., $dt_{\rm acc} =$ 5 minutes.

On the other hand, back-extrapolation of the kinematical curve of the shock signatures fits well with the impulsive phase of the flare. Similarly to all other events analyzed in this paper, the associated flare was quite impulsive, i.e., the flare impulsive phase lasted about 4 minutes. This is a strong indication of the impulsive increase of the pressure which favors the blast wave theory and a flare-generated shock wave. Therefore, we conclude that this shock wave was probably generated by the flare and not driven by the CME.

3.4. The 2005 January 21 Event

3.4.1. Characteristics of the Flare and Radio Event

The CME/flare event on 2005 January 21 was related to a *GOES* M1.7 flare from the NOAA AR 10720 (19°N 81°W). The flare started at 10:12 UT and attained its maximum at 10:16 UT (Figure 1(h) and Table 1).

During the time interval 10:14:30–10:16:00 UT, radio observations in the microwave range (2.0–4.5 GHz) show intense type-III-like bursts that indicate the impulsive phase of the associated flare. In the metric range, the continuation of the radio emission in a form of weak type-III-like bursts is observed. The AIP and Phoenix-2 dynamic spectra show metric type II bursts in the frequency range of 490–100 MHz, lasting from 10:16:00 to 10:19:00 UT.

We identified two homologous metric type II bursts (denoted here as first and second type II burst). Figure 1(d) shows well-defined harmonic bands of type II bursts observed in the frequency range 490–160 MHz. A weak and patchy drifting emission observed at lower frequencies (170–100 MHz) was probably the fundamental band of the first type II burst. We assume that, due to a rather weak intensity of the second type II burst, its fundamental band was not observed. The morphological similarity between the harmonic bands of the two type II bursts imply that the shock waves propagated through the same coronal structures. This conclusion is confirmed by the radio imaging. We found that the position of the NRH source for the first type II burst was at the heights of 0.17 and 0.26 $R_\odot$ at 237 and 327 MHz, respectively. The height of the NRH source for the second type II burst was 0.20 and 0.26 $R_\odot$ at 237 and 327 MHz, respectively. Since positions of the radio sources are nearly the same for both bursts, it can be concluded that the two shock waves, one after the other, passed through the same plasma. Thus, the possibility that the emission of these two type II bursts comes from different parts of the same shock wave can be excluded. Both type II bursts showed a very fast drift

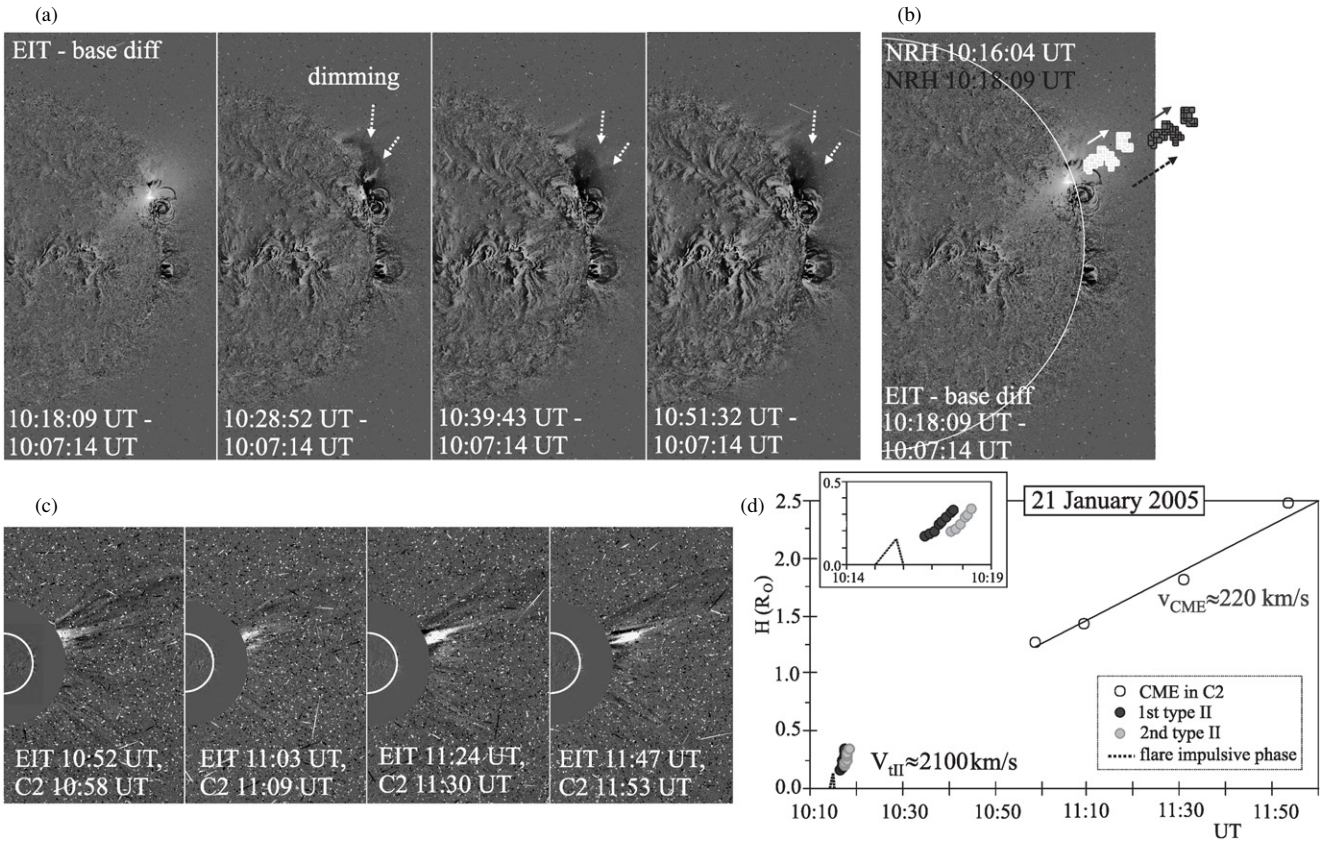

Figure 6. CME/flare event on 2005 January 21. (a) Base difference EIT images show a dimming (marked by arrows). (b) Centroids of the NRH type II burst sources at 237, 327, 408, and 432 MHz (marked with white circles) overlaid on the closest EIT image (10:18:09 UT). The propagation of the NRH sources indicates the direction of the shock wave propagation. The radio sources correspond to the harmonic band of the first type II burst. The corrected positions of the NRH sources (marked with black circles) take into account the time difference between the shock signatures and the EIT image, as well as the shock velocity. (c) LASCO C2 running-difference images combined with temporally closest EIT running-difference images showing propagation of the narrow CME. (d) Kinematics of the CME compared with signatures of the shock waves and the flare impulsive phase.

rate of $df/dt = 2.4$ MHz s^{-1}, which indicates similar shock velocities.

The starting frequency of the second type II burst was about 380 MHz which is significantly lower than the starting frequency of the first type II burst (490 MHz). Therefore, the first type II burst was imaged by the NRH at its four observing frequencies (432, 408, 327, and 237 MHz) and the second type II burst only at two lower frequencies. This exceptionally good coverage provides us with a unique opportunity to examine density changes along the propagation path of the shock wave. It was found that, for both type II bursts, density changes rather smoothly following the density distribution of 3.8× Saito. When the most extreme positions of the NRH sources at all four observing frequencies were considered, we obtained the densities of 3.4× Saito and 4.2× Saito. The error on the shock wave speed estimated using these two different density models is about ±80 km s^{-1} (Figure 2). Applying the obtained density distribution and type II band split (BDW ≈ 0.27), for both type II bursts, the shock velocity, Alfvén velocity and Alfvén Mach number were found to be 2100 km s^{-1}, 1300 km s^{-1}, and 1.6, respectively.

3.4.2. CME and Associated Dynamics in the Low Corona

In this CME/flare event, base difference EIT (195 Å) images show a rather large dimming (starting at 10:28:52 UT) in the northward direction from the flare site (Figure 6(a)). The angular position of dimming, which appears 30 minutes before the first observation of the CME in the LASCO C2 field of view, coincides with the later observed CME position confirming that the dimming was a signature of the CME liftoff.

Figure 6(c) shows a very narrow CME first observed at the height of $H = 1.4\,R_\odot$, propagating in the LASCO C2 field of view at a velocity of about 220 ± 50 km s^{-1}. The error bar of the CME speed was estimated taking into consideration the error or ±2 pixels, i.e., ±0.02 $R_\odot$ in the LASCO C2 field of view. The error of ±0.02 $R_\odot$ is smaller than the size of the symbols in Figure 6(d). A slightly higher mean CME speed of 273 km s^{-1} was reported in the LASCO CME catalog (Yashiro et al. 2004). Unfortunately, we do not have observations of the CME at lower heights, so it was not possible to measure the acceleration phase of the CME and to use the theoretical model by Žic et al. (2008).

Nevertheless, one can consider some of the possible scenarios. In a bow-shock scenario, in order to drive the observed shock we expect that the CME should have velocity comparable to the velocity of the shock wave, i.e., about 2000 km s^{-1}. In contrast, the CME had a speed of only 220 km s^{-1}, which implies that the CME probably was not driving the shock wave. Furthermore, a recent study of well-observed CMEs and type II bursts by Gopalswamy et al. (2009) has shown that heights at which CME-driven shocks form are around 0.5 $R_\odot$, which is significantly larger than the observed heights in this event (around 0.2 $R_\odot$). The scenario of the CME as a driver of the observed shock seems therefore unlikely.

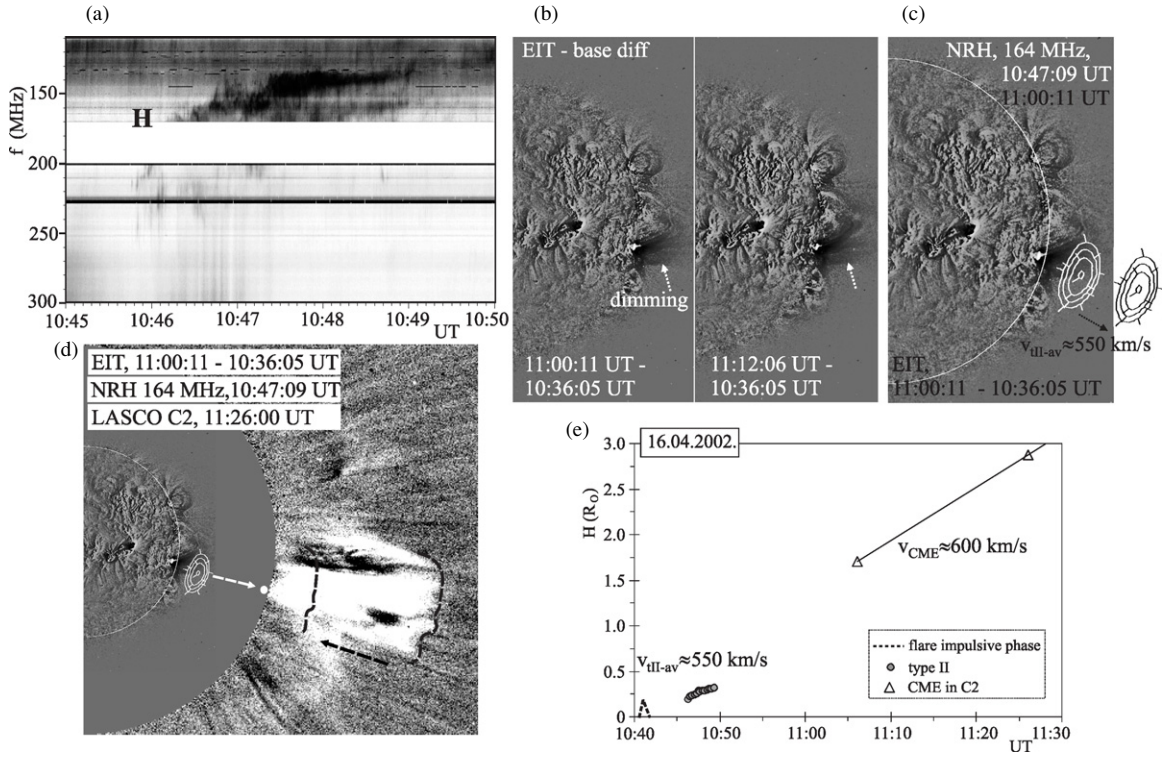

Figure 7. (a) AIP dynamic spectrum showing the type II burst recorded on 2002 April 16. (b) EIT base difference images showing a coronal dimming (marked by white arrow). (c) The NRH radio source at 10:47:09 UT overlaid on the temporally closest EIT image. (d) The temporally closest NRH (10:47:09 UT), EIT (11:00:11–10:36:06 UT), and LASCO C2 (11:26:00–11:06:00 UT) image overlaid. The position of the CME leading edge and the position of the NRH source were corrected for the time difference with the EIT image. The corrected positions (indicated with arrows) were estimated using the average shock speed and CME velocity. (e) The CME dynamics compared with the signatures of the shock wave and the flare impulsive phase.

Let us assume, for the sake of argument, that the CME was the driver of the shock wave. First, we consider that the observed heights of the shock and driving CME are comparable, i.e., that the standoff distance between the shock and the CME close to the Sun is rather small (Gopalswamy et al. 2009). Second, we assume that the acceleration phase of the CME is well synchronized with the impulsive phase of the flare, i.e., the acceleration of the CME ceases near the peak time of the SXR flare (Zhang et al. 2001; Temmer et al. 2008). Then the CME should have reached a velocity comparable to 2000 km s^{-1} at the height $H \leqslant 0.2\,R_{\odot}$, before the type II bursts appeared. After reaching the maximum speed, the CME should have decelerated in about 40 minutes to 200 km s^{-1} (LASCO C2 field of view, height of about $H = 1.4\,R_{\odot}$). In such a scenario, the average deceleration should be as large as -750 m s^{-2}, which is much higher than the generally observed value (Vršnak 2001). A typical CME deceleration is about -20 m s^{-2} (Gopalswamy et al. 2001), and only in extreme cases is it found to reach values of about -150 m s^{-2} (Vršnak 2001; Vršnak et al. 2004b). Thus, we again conclude that it is very unlikely that this CME was a driver of the shock. On the other hand, since back-extrapolation of the type II source kinematics fits well to the flare impulsive phase (lasting for only 2 minutes), we conclude that the shock wave was probably ignited by the flare.

3.5. An Inconclusive Event: 2002 April 16

The CME/flare event on 2002 April 16 was related to a *GOES* C9.3 flare from the NOAA AR 9904 (19°N 81°W). The flare started at 10:37 UT and attained its peak at 10:44 UT (Table 1).

Type III radio bursts were recorded during the impulsive phase of the flare (10:41–10:42 UT), propagating from the metric to kilometric range. The AIP dynamic spectrum (Figure 7(a)) shows a well-defined harmonic band of the type II burst during the time interval 10:46–10:50 UT in the frequency range 250–100 MHz. The average frequency drift of the type II burst was about $df/dt \sim 0.30$ MHz s^{-1}. Analyzing the evolution of the dominant NRH source, we obtained somewhat low densities, corresponding to the coronal density model of 1.3× Saito (with 1.2× Saito and 1.4× Saito as extreme values). Using the obtained density profiles, we estimated the average shock velocity to be about 550 ± 20 km s^{-1}. We note that the change of the drift rate of the type II burst indicates that the shock might have been decelerating (from about 1000 to about 300 km s^{-1}). The other explanation is that the density changes much more steeply than in the Saito density model, producing large changes of the instantaneous frequency drift. Using the well-defined band split (BDW $\approx$ 0.27) of the type II burst (Figure 7(a)), we estimated the Alfvén velocity and the Alfvén Mach number to be 330 km s^{-1} and 1.6, respectively.

The EIT (195 Å) observations show a trans-equatorial loop system connecting NOAA ARs 9904 and 9905 with active regions on the northwest limb. The eruption was accompanied with a coronal dimming (Figure 7(b)), slightly in the northward direction from the flare site and along the trans-equatorial loops. The dimming was first observed at 11:00:11 UT and the associated CME at 11:06 UT (in the LASCO C2 field of view). The LASCO CME catalog (Yashiro et al. 2004) reports a CME speed of 496 km s^{-1}, which is somewhat smaller than the velocity of the CME obtained in this study. We found

that the CME speed was about 600 ± 30 km s^{-1} (the error of ±2 pixels, i.e., ±0.02 $R_\odot$ in the LASCO C2 field of view) during the time interval closest to the appearance of the shock signatures and slowly decelerated to a rather constant velocity of 500 km s^{-1} in the LASCO field of view. In this CME/flare event, the CME speed is comparable to the velocity of the shock wave (Figure 7(e)).

The dynamics of the CME and the associated shock wave indicate that the shock might have been CME-driven. On the other hand, shock signatures are rather well correlated with the impulsive phase of the flare. Additionally, a possible decrease of the shock velocity indicates that the shock might have been flare-ignited.

Figure 7(d) shows the temporally closest EIT and LASCO C2 images overlaid with the position of the NRH source corresponding to the harmonic band of the type II burst. The average shock speed (550 km s^{-1}) and CME velocity were used to extrapolate the position of the shock and CME leading edge to the time of the EIT image. The corrected position of the shock wave signature (the white dot in Figure 7(c)) is about half-solar radii behind the corrected position of the leading edge of the CME (black dashed line), which is not in agreement with the idea of the CME-driven shock wave. However, the correction of the distance between the shock signatures and the CME leading edge was performed using average CME and shock velocities. This is rather ambiguous since it seems that both the CME speed and the shock wave velocity are changing (from 600 to 500 km s^{-1} and from 1000 to 300 km s^{-1}, respectively). We note that, although the close location of the type II burst source close to the CME leading edge does not completely prove that the shock was CME-driven, it gives a very strong indication of a CME-driven shock. Due to all listed uncertainties it is not possible to unambiguously determine the origin of the coronal shock wave associated with the 2002 April 16 CME/flare event.

Note that the velocity of the CME was found to be slightly larger than reported in the CME catalog and therefore also larger than that imposed in the selection criteria. Moreover, the CME speed in this event is comparable to the shock speed and is noticeably larger that in the events discussed in the previous sections. It is possible that this CME/flare event with an intermediate speed CME belongs to a different class of events where it is not possible to unambiguously determine the shock driver.

4. SUMMARY AND CONCLUSIONS

In this paper, we analyzed a set of well-observed CME/flare events associated with metric type II bursts, i.e., shock signatures (for which radio-source positions were available through NRH observations), and rather slow CMEs. The aim of the study was to determine whether shock waves were CME-driven or flare-generated, and in that way to test the hypothesis that all coronal shocks are CME-driven (Cliver et al. 2004).

We focused on the possibility that the impulsive energy release in a flare ignites the shock wave that results in the type II radio burst. Therefore, an important criterion in the event selection is the association of the fast shock wave with a rather slow CME ($v_{\rm CME} \leqslant 500$ km s^{-1}). In order to minimize projection effects, we selected only events originating close to the limb.

The origin of shock waves was discussed separately for each studied CME/flare event. We found that out of five analyzed type II bursts, four should be considered as signatures of flare-ignited shocks (Section 3). For one event it was not possible to give a conclusive answer due to a close temporal association of the CME, flare, and shock signatures. An additional uncertainty was introduced by the comparable velocity of the CME and the shock wave.

We now summarize our conclusions and list the common characteristics of CME/flare events associated with coronal shock waves probably generated by flares. Our main findings are as follows.

1. The shock wave velocity strongly exceeds the speed of the associated CME, sometimes even by an order of magnitude.
2. Shock formation heights obtained from radio imaging (around 0.2 $R_\odot$) are significantly smaller than the heights of CME-driven shock waves (around 0.5 $R_\odot$) reported by Gopalswamy et al. (2009).
3. The analytical MHD model by Žic et al. (2008) predicts much larger heights (about 1 $R_\odot$) of the CME-driven shock formation than the observed heights of type II bursts. Additionally, the modeled shock formation occurs long (more than 10 minutes) after the passage of the type II burst.
4. All studied CME/flare events are associated with very impulsive flares (impulsive phase lasting only a few minutes). This is a good indication of a strong, impulsive increase of the pressure and flare-generated blast wave.
5. There is a very good temporal association of shock waves with the impulsive phase of the corresponding flare.

Based on the presented results, we conclude that a particular class of the CME/flare events with flare-generated shock waves does exist. We do not claim that all coronal shocks are flare-generated; we show that some of the coronal shock waves are probably not CME-driven but generated by flares. This result is contrary to the conclusion by Cliver et al. (2004) that all coronal shocks are CME-driven. However, we do not exclude a possibility that the presence of a mass ejection, i.e., CME, might be a necessary condition for the shock formation (see, e.g., Vršnak et al. 2006).

EIT and LASCO data have been used courtesy of the *SOHO*/EIT and *SOHO*/LASCO consortiums, respectively. The CME catalog is generated and maintained at the CDAW Data Center by NASA and The Catholic University of America in cooperation with the Naval Research Laboratory. *SOHO* is a project of international cooperation between ESA and NASA. We are grateful to the staff of the Nançay Radioheliograph (Paris Observatory) and ETH Zurich for their open data policy. We acknowledge Henry Aurass for the AIP spectral data. J.M. and B.V. acknowledge funding from The European Community's Seventh Framework Programme (FP7/2007-2013) under grant agreement no. 218816 (SOTERIA). We are grateful to N. Gopalswamy for the helpful discussions and to the referee for constructive comments and suggestions.

REFERENCES

Aurass, H., Klein, K., & Mann, G. 1994, in Solar Dynamic Phenomena and Solar Wind Consequences, ed. J. J. Hunt (ESA SP-373; Noordwijk: ESA), 95

Brown, J. C., & Kontar, E. P. 2005, Adv. Space Res., 35, 1675

Brueckner, G. E., et al. 1995, Sol. Phys., 162, 357

Ciaravella, A., Raymond, J. C., Kahler, S. W., Vourlidas, A., & Li, J. 2005, ApJ, 621, 1121

Cliver, E. W., Nitta, N. V., Thompson, B. J., & Zhang, J. 2004, Sol. Phys., 225, 105

Delaboudinière, J.-P., et al. 1995, Sol. Phys., 162, 291

Duncan, R. A. 1979, Sol. Phys., 63, 389
Gopalswamy, N., Yashiro, S., Kaiser, M. L., Howard, R. A., & Bougeret, J.-L. 2001, J. Geophys. Res., 106, 29219
Gopalswamy, N., Yashiro, S., Xie, H., Akiyama, S., Aguilar-Rodriguez, E., Kaiser, M. L., Howard, R. A., & Bougeret, J. 2008, ApJ, 674, 560
Gopalswamy, N., et al. 2009, Sol. Phys., 259, 227
Kerdraon, A., & Delouis, J.-M. 1997, in Coronal Physics from Radio and Space Observations, ed. G. Trottet (Lect. Notes Phys. 483; Berlin: Springer), 192
Magdalenić, J., Vršnak, B., Pohjolainen, S., Temmer, M., Aurass, H., & Lehtinen, N. J. 2008, Sol. Phys., 253, 305
Magun, A., Stewart, R. T., & Robinson, R. D. 1975, PASA, 2, 367
Mancuso, S., Raymond, J. C., Kohl, J., Ko, Y.-K., Uzzo, M., & Wu, R. 2002, A&A, 383, 267
Mann, G., Aurass, H., Voigt, W., & Paschke, J. 1992, in Coronal Streamers, Coronal Loops, and Coronal and Solar Wind Composition, ed. C. Mattok (ESA SP-348; Noordwijk: ESA), 129
Mann, G., Classen, T., & Aurass, H. 1995, A&A, 295, 775
Mann, G., Jansen, F., MacDowall, R. J., Kaiser, M. L., & Stone, R. G. 1999, A&A, 348, 614
Mann, G., Klassen, A., Classen, H., Aurass, H., Scholz, D., MacDowall, R. J., & Stone, R. G. 1996, A&AS, 119, 489
Maričić, D., Vršnak, B., Stanger, A. L., Veronig, A. M., Temmer, M., & Roša, D. 2007, Sol. Phys., 241, 99
McLean, D. J. 1973, PASA, 2, 222
Messmer, P., Benz, A. O., & Monstein, C. 1999, Sol. Phys., 187, 335
Nelson, G. J., & Melrose, D. B. 1985, in Type II Bursts, Solar Radiophysics: Studies of Emission from the Sun at Metre Wavelengths, ed. D. J. McLean & N. R. Labrum (Cambridge: Cambridge Univ. Press), 333
Neupert, W. M. 1968, ApJ, 153, L59
Newkirk, G. J. 1961, ApJ, 133, 983
Oh, S. Y., Yi, Y., & Kim, Y. H. 2007, Sol. Phys., 245, 391
Pohjolainen, S. 2008, A&A, 483, 297
Priest, E. R. 1982, Solar Magnetohydrodynamics (Dordrecht: Reidel)
Raymond, J. C., et al. 2000, Geophys. Res. Lett., 27, 1439
Reiner, M. J., Kaiser, M. L., Gopalswamy, N., Aurass, H., Mann, G., Vourlidas, A., & Maksimovic, M. 2001, J. Geophys. Res., 106, 25279
Saito, K., Makita, M., Nishi, K., & Hata, S. 1970, Ann. Tokyo Astron. Obs., 12, 51
Sheridan, K. V., McLean, D. J., & Smerd, S. F. 1973, Astrophys. Lett., 15, 139
Smerd, S. F., Sheridan, K. V., & Stewart, R. T. 1974, in IAU Symp. 57, Coronal Disturbances, ed. G. A. Newkirk (Dordrecht: Reidel), 389
Smerd, S. F., Sheridan, K. V., & Stewart, R. T. 1975, Astrophys. Lett., 16, 23
Temmer, M., Veronig, A. M., Kontar, E. P., Krucker, S., & Vršnak, B. 2010, ApJ, 712, 1410
Temmer, M., Veronig, A. M., Vršnak, B., Rybák, J., Gömöry, P., Stoiser, S., & Maričić, D. 2008, ApJ, 673, L95
Veronig, A., Vršnak, B., Dennis, B. R., Temmer, M., Hanslmeier, A., & Magdalenić, J. 2002, A&A, 392, 699
Vršnak, B. 2001, Sol. Phys., 202, 173
Vršnak, B., Aurass, H., Magdalenić, J., & Gopalswamy, N. 2001, A&A, 377, 321
Vršnak, B., & Cliver, E. W. 2008, Sol. Phys., 253, 215
Vršnak, B., & Lulić, S. 2000, Sol. Phys., 196, 157
Vršnak, B., Magdalenić, J., Aurass, H., & Mann, G. 2002, A&A, 396, 673
Vršnak, B., Magdalenić, J., & Zlobec, P. 2004a, A&A, 413, 753
Vršnak, B., Maričić, D., Stanger, A. L., Veronig, A. M., Temmer, M., & Roša, D. 2007, Sol. Phys., 241, 85
Vršnak, B., Ruždjak, D., Sudar, D., & Gopalswamy, N. 2004b, A&A, 423, 717
Vršnak, B., Warmuth, A., Temmer, M., Veronig, A., Magdalenić, J., Hillaris, A., & Karlický, M. 2006, A&A, 448, 739
Wild, J. P. 1950, Aust. J. Sci. Res. A: Phys. Sci., 3, 399
Wild, J. P., Murray, J. D., & Rowe, W. C. 1954, Aust. J. Phys., 7, 439
Yashiro, S., Gopalswamy, N., Michalek, G., St. Cyr, O. C., Plunkett, S. P., Rich, N. B., & Howard, R. A. 2004, J. Geophys. Res.: Space Phys., 109, 7105
Zhang, J., & Dere, K. P. 2006, ApJ, 649, 1100
Zhang, J., Dere, K. P., Howard, R. A., Kundu, M. R., & White, S. M. 2001, ApJ, 559, 452
Žic, T., Vršnak, B., Temmer, M., & Jacobs, C. 2008, Sol. Phys., 253, 237
Zlotnik, E. Y., Klassen, A., Klein, K., Aurass, H., & Mann, G. 1998, A&A, 331, 1087